ISSN 1027-5495. Functional Materials, 30, No.2 (2023), p. 197-205.
doi:https://doi.org/10.15407/fm30.02.197

Interaction of composite ceramics based on zirconium diboride with high temperature alloys based on iron and nickel

G.Zhunkovskii, O.Grigoriev, D.Vedel

Frantsevich Institute for Problems of Materials Science,
National Academy of Sciences of Ukraine, 3 Krzhyzhanovsky Str.,
03142 Kyiv, Ukraine

Received January 20, 2023

The solid-phase interaction and contact melting of the ZrB_2-15 vol. % $MoSi_2$ with Fe alloy, and Ni base-alloys were carried out. It has been established that in the composite-Fe alloy system up to a temperature of 1200°C in vacuum, there is no chemical interaction with the formation of new phases at the contact boundary. Changes occur only in the near-contact zone of the composite: $MoSi_2$ disappears with the formation of pores in its place, and from the side of the metal there is a zone enriched with silicon. Similar processes are observed during solid-phase interaction in the systems ZrB_2-15 vol. % $MoSi_2$–Ni base alloys. However, in these systems, in addition to the diffusion of silicon from the composite into the alloy, counter diffusion of chromium from the metal to the contact boundary and into the composite occurs, followed by interaction and the formation of a layer of a new Cr_2B phase. At temperatures above 1200°C, contact melting occurs and a multilayer structure is formed over the cross section of contacting pairs. In this case, for the system with steel, the main phases are the base of stainless steel saturated with silicon and zirconium and the phases: $(Fe,Cr)_2B$, $(Ni,Fe)_{16}Si_7Zr_6$, $(Mo,Cr,W)B_2$ and ZrB_2. In the nichrome alloy system, the main phases are silicon alloyed nickel, Ni_3Si, $Ni_{16}Si_7Zr_6$ silicides and $(Cr,Mo)_2B$, $(Mo,Cr,W)B_2$ and ZrB_2 borides. These studies demonstrate that in contact pairs ZrB_2-15 vol. % $MoSi_2$ — an alloy based on iron and nickel, the maximum operating temperature is 1000°C. In the case of more severe operating modes with temperatures of 1200°C and above, it is necessary to create barrier layers at the contact boundary to prevent possible diffusion and contact melting of the contacting pairs.

Keywords: Zirconium diboride, molybdenum disilicide, contact interaction.

Взаємодія композиційної кераміки на основі дибориду цирконію з жаростійкими сплавами на основі заліза та нікелю. *Г.Жунківський, О.Григорьев, Д.Ведель*

Досліджено твердофазну взаємодію і контактне плавлення композиту ZrB_2 об. % $MoSi_2$ з Х18Н10Т, ВХ4Л та ніхромом. Встановлено, що до температури 1200°С в вакуумі в системі композит-нержавіюча сталь хімічної взаємодії з утворенням на границі контакту нових фаз відсутня. Зміни відбуваються тільки в приконтактній зоні композиту: зникає $MoSi_2$ з утворенням на його місці пор, а зі сторони металу виникає зона збагачена на кремній. Аналогічні процеси спостерігаються при твердофазній взаємодії в системах ZrB_2 об. % $MoSi_2$ — ВХ4Л чи ZrB_2 об. % $MoSi_2$ — Ni–20Cr. Але в цих системах, крім дифузії кремнію із композита в сплав, має місце зустрічна дифузія хрому із метала на границю контакту і в композит з послідуючою взаємодією і формуванням прошарку нової фази Cr_2B. За температур вищих за 1200°С відбувається контактне плавлення та формування багатошарової структури по перерізу контактуючих пар. Основними фазами при цьому для системи зі сталлю є насичена кремнієм і цирконієм основа нержавіючої сталі та фази: $(Fe,Cr)_2B$, $(Ni,Fe)_{16}Si_7Zr_6$, $(Mo,Cr,W)B_2$ і ZrB_2. В системі з ніхромовим сплавом, основними фазами є легований кремнієм нікель,

силіциди Ni_3Si, $Ni_{16}Si_7Zr_6$ та бориди $(Cr,Mo)_2B$, $(Mo,Cr,W)B_2$ і ZrB_2. Проведені дослідження демонструють, що в контактних парах ZrB_2 об. % $MoSi_2$ — сплав на основі заліза та нікелю максимальна робоча температура становить 1000°С. У випадку більш жорстких режимів роботи з температурами 1200°С і вище необхідно створювати на границі контакту бар'єрні шари для запобігання можливої дифузії та контактного плавлення контактуючих пар.

1. Introduction

Physical, chemical and mechanical properties and some areas of application of zirconium diboride (ZrB_2) are presented in [1, 2]. Single-phase ZrB_2 or composites based on ZrB_2 are used as high temperature ceramics in protective atmosphere [3–5] or ceramics operating at high temperature in oxidative atmosphere [6–8]. The base line composite based on zirconium diboride is ZrB_2-10–20) vol. % $MoSi_2$ [9–14]. This composition combines high oxidation and thermal stability that makes it one of the most promising materials for application at high temperatures, as was shown in [15–17].

However, the success of using ceramics is associated not only with its high temperature properties. Also, ceramic elements are connected to parts of structures made of metal or metal alloys [18, 19]. Therefore, the interaction of ceramic elements with the material of structural parts during operation is no less important than their high-temperature properties. It is one of the main limiting factors, which, along with heat resistance, determine the temperature of operational capabilities of the structure.

In our previous works, we investigated the interaction between pure zirconium diboride with chromium, nickel, nichrome, iron and their alloys [20–23]. It has been shown that solid-phase interaction does not occur up to 1200°C in the systems with pure Fe or Ni [20, 21]. However, during the contact of ZrB_2 with Cr, Ni–Cr, and X18H10T, the interaction occurs with the formation of a layer of a new phase — Cr_2B [20, 22, 23]. At temperatures above 1200°C, liquid-phase interaction occurs with the formation of new phases in the form of eutectics.

The purpose of this work is to investigate interactions between a composite material ZrB_2-15 vol. % $MoSi_2$ with industrial representatives of high-temperature alloys based on iron and nickel. They are iron-based alloys with X18N10T and alloys based on nickel and chromium: VH4L-VI and Ni-20 wt. % Cr, respectively.

2. Experimental

Rolled steel X18N10T, VH4L-VI, NiCr (Ni-20 wt. % Cr), powders of zirconium diboride and molybdenum disilicide were used as raw materials. The chemical compositions are presented in Table 1.

The ZrB_2-15 vol.% $MoSi_2$ ceramic composites were hot-pressed for 30 min at a temperature of 1850°C and a pressure of 30 MPa. Details of hot pressing are presented in [16]. Ceramic and metal alloy samples with dimensions of 4 mm×4 mm×3 mm were polished to a surface finish of 0.63 and brought into contact.

The annealing was carried out in a SShVL-0.6.2/25 vacuum furnace in the temperature range of 1200–1450°C with exposure from 1 to 5 h at a residual pressure of 10^{-3} Pa.

The microstructures were studied on an electronic microscope (TESCAN Mira 3) equipped with an Energy Dispersive Spectroscopy (EDS) detector (Oxford X-Max).

3. Results

The microstructure and EDS results of the contact zones of the annealed couples are shown in Fig. 1. No chemical interaction with the formation of new phases was found at the contact boundary for the X18N10T-ZrB_2-15 vol.% $MoSi_2$ system at

Table 1. Chemical composition of raw materials

Material	Element composition, wt. %										
	Zr	Cr	Ni	Fe	Mn	Mo	W	Ti	Si	C	B
ZrB_2	base	–	–	0.1	–	–	–	–	–	1.2	17–19
$MoSi_2$	–	–	–	–	–	base	–	–	35–37	–	–
X18H10T	–	17–19	9–11	base	1–2	–	–	0,6	0.8	0.12	–
VH4L–VI	–	32–35	base	0.5	–	2.3–3.5	4.3–5.5	0.7–1.3	0.1	0.1	
Ni–20 Cr		23–27	base		1.5						

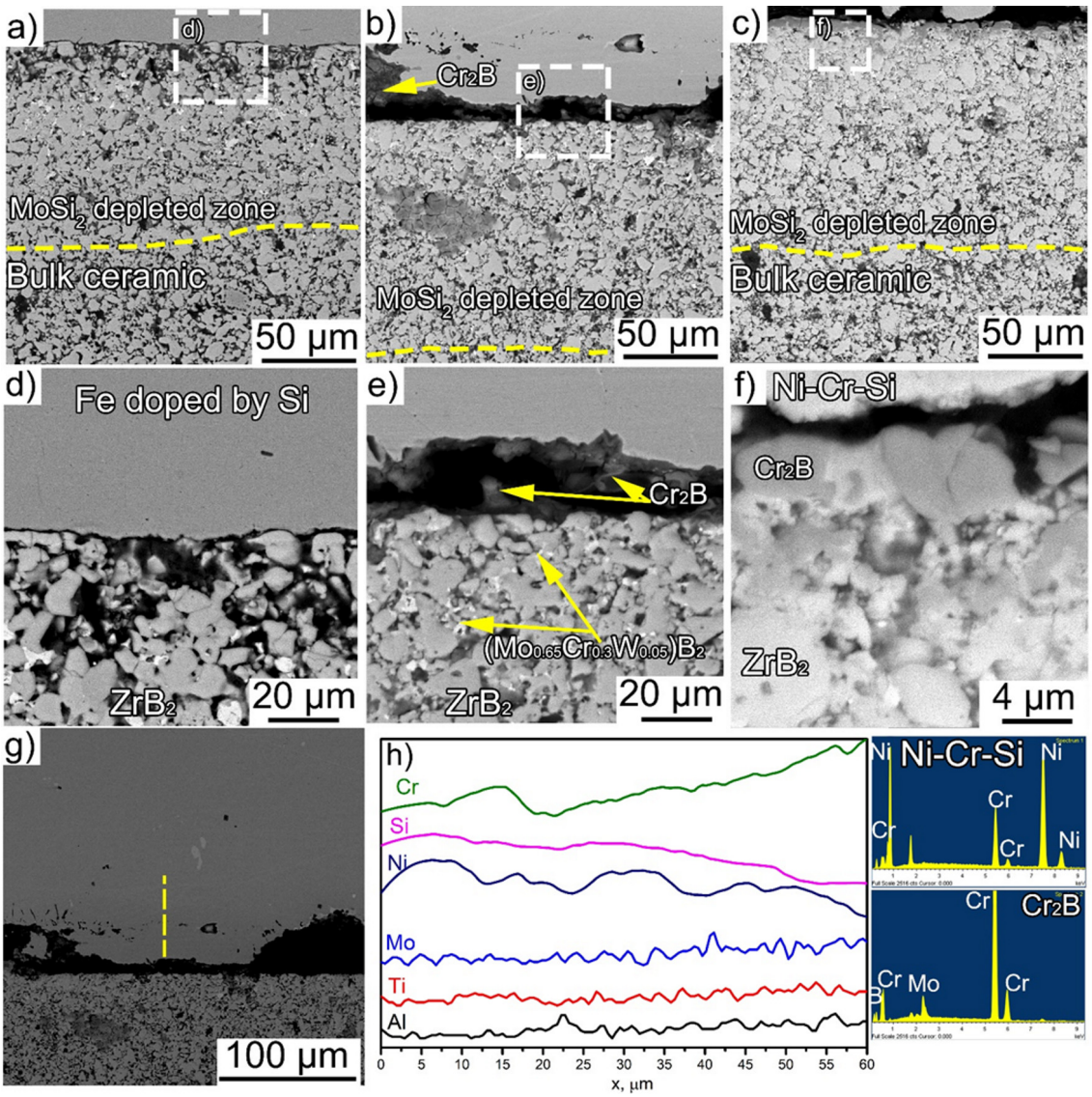

Fig. 1. Microstructure of contact couples: (a, d) X18H10T-(ZrB_2-15 wt. % $MoSi_2$), (b, e) VH4L-VI-(ZrB_2-15 wt. % $MoSi_2$, (c, f, g) (NiCr)-(ZrB_2-15 wt. % $MoSi_2$), (g) distribution of elements along the line for the VH4L-VI-(ZrB_2-15 wt. % $MoSi_2$) couple.

1200°C (Fig. 1a, d). However, the phase composition of the ceramics has partially changed. Near the contact boundary, a layer depleted in $MoSi_2$ appears, the thickness of which increases with increasing temperature and duration of annealing.

The solid-phase interaction of the ZrB_2-15 wt.% $MoSi_2$ with NiCr and VH4L-VI alloys occurs in a similar way. The main difference is active diffusion from the alloys to the contact zone and formation of a layer of Cr_2B or a complex diboride (Mo, Cr, W) B2 (Fig. 1b, d). As in the case of the ZrB2-X18N10T couple, silicon interacts with the contact surface of the metal part and diffuses into its depth, which is confirmed by the EDS data (Fig. 1c). The diffusion of silicon into nickel is also confirmed by the results of studying the interaction of nickel with molybdenum disilicide [25].

Zhunkovskii et al. showed [26] that chromium is one of the most active sintering additions for borides. Therefore, the presence of the $(Mo,Cr,W)B_2$ phase in the porous layer led to the restoration of its density due to activated sintering processes (Fig. 1a, b, c). It should be noted that, the destruction of the interaction zone in the NiCr–ZrB_2-15 wt.% $MoSi_2$ and VH4L-VI-ZrB_2-15 wt.% $MoSi_2$ couples was due to a large mismatch between thermal expansion coefficients (TEC) of the alloys ($\alpha_{Fe} = 10.7 \cdot 10^{-6}$ °C^{-1} [27], $\alpha_{Ni} = 13.2 \cdot 10^{-6}$ °C^{-1} [27]) and brittle ceramics Cr_2B ($\alpha_{Cr2B} = 8.2 \cdot 10^{-6}$ °C^{-1} [28]), Fig. 1.

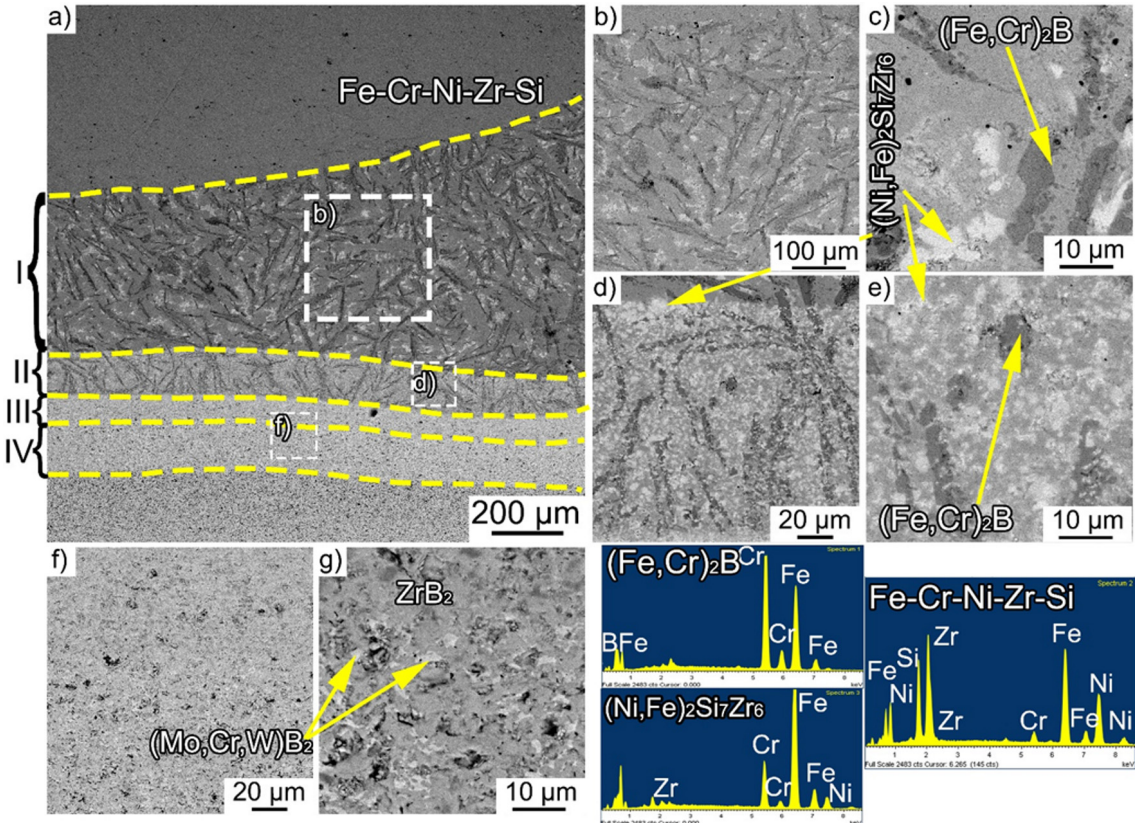

Fig. 2. Microstructure of the cross-section and phase composition of the X18H10T-(ZrB_2-15 wt. % $MoSi_2$) contact couple after an annealing at 1200°C for 3 hours: (a) general view, (b, c) region with $(Ni,Fe)_2Si_{17}Zr_6$ and $(Fe,Cr)_2B$ phases, (d, e) zone with fine-grained $(Ni,Fe)_2Si_{17}Zr_6$ phase, (f, g) zone adjacent to ceramic.

At temperatures more 1200°C, a liquid phase was observed (Figs. 2–4). That is, contact melting of interacting materials has taken place. At the same time, the slow, smooth hardening of the alloy with chemical accumulation, apparently, occurred along the cut of the cold zone. In this case, an alloy is formed with a changing phase and chemical composition and, accordingly, a microstructure over the cross section of the contact zone. Chemical and phase compositions of the contact zone are presented in Table 2.

The cross section and phase composition of the X18H10T-ZrB_2-15 % $MoSi_2$ couple after liquid phase interaction at a temperature more than 1200°C are shown in Fig. 2. As a result of the interaction between the components, the microstructure can be conditionally divided into 4 zones, smoothly passing one into another. Beginning from the Si-enriched metal, the first zone is a ~ 460 μm thick composite with a stainless steel matrix with reinforcing components $(Fe,Cr)_2B$ and $(Ni,Fe)_{16}Si_7Zr_6$ (Fig. 2b). In this case, the ratio between the phases in the direction of the ceramics increases to

Table 2. Changes in the phase and chemical composition of the contact zone after annealing the couple at ~ 1200°C for 3 hours

Contact couple	(ZrB_2-15 % $MoSi_2$) depleted on $MoSi_2$, μm	Cr_2B zone, μm	The thickness of the Si-enriched metal zone, μm
(ZrB_2-15 % $MoSi_2$)-X18H10T	~ 108	0	~ 32 (~ 3 at.%)*
(ZrB_2-15 % $MoSi_2$)-VH4L-VI	~ 120	~ 10	~ 45 (~ 4.5 at.%)**
(ZrB_2-15 % $MoSi_2$)–NiCr	~ 118	~ 10	~ 40 (~ 5 at.%)**

* Fe–Si (T_e ~ 1212°C) ** Ni–Si (T_e ~ 1143°C)

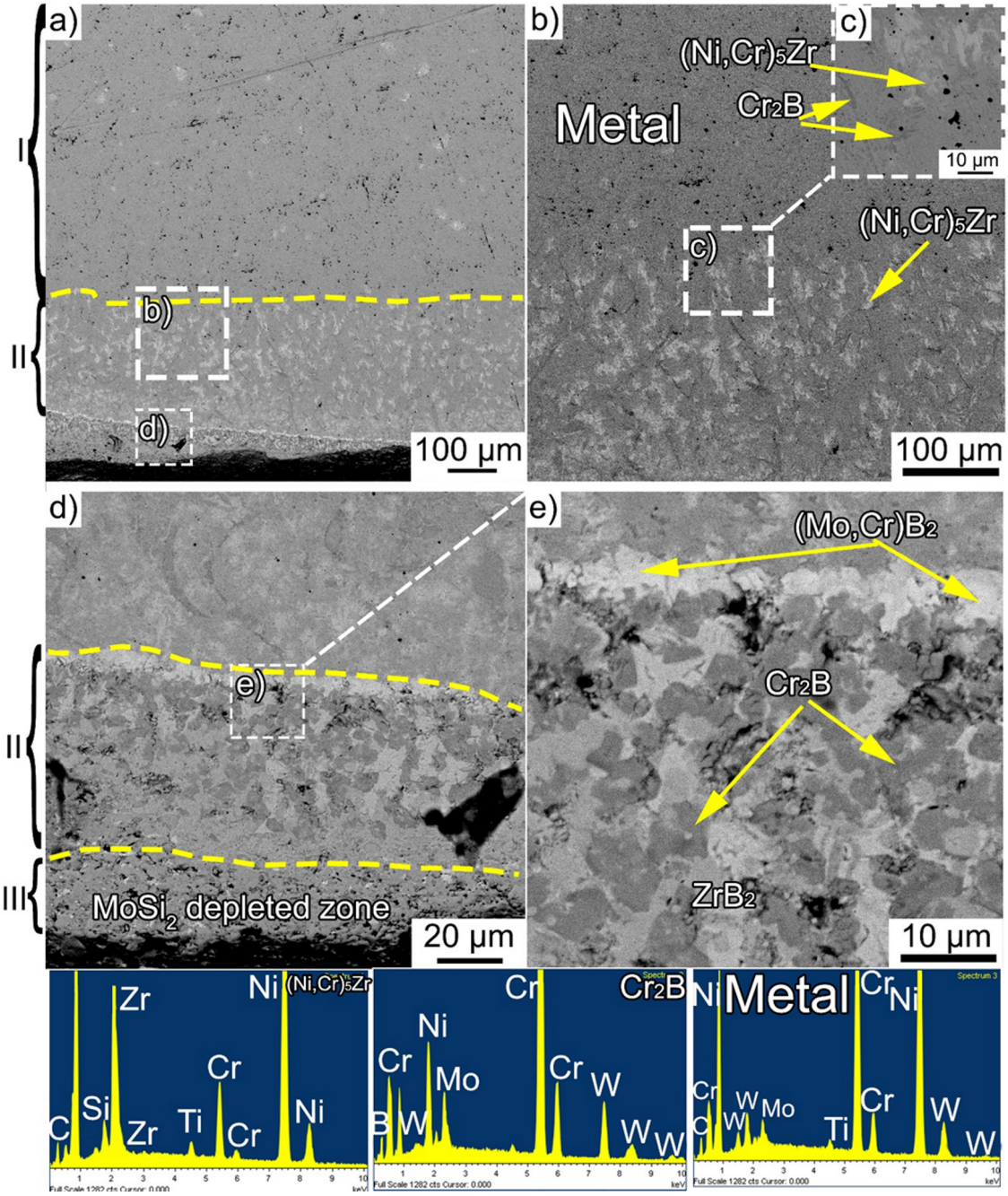

Fig. 3. Cross-section microstructure and phase composition of the VH4L-VI-(ZrB_2-15 wt. % $MoSi_2$) contact couple after annealing at 1200°C for 3 hours: (a) general view, (b, c) region with $(Ni,Cr)_5Zr$ and Cr_2B phases, (d, e) zone adjacent to ceramic with $(Mo,Cr)B_2$ and Cr_2B phases.

$(Ni,Fe)_{16}Si_7Zr_6$. In the second zone with a thickness of ~ 128 μm, the phase composition does not change, but the amount of the silicide phase $(Ni,Fe)_{16}Si_7Zr_6$ becomes larger (Fig. 2d,e). The third zone ~ 44 μm thick adjacent to the ceramics consists of ZrB_2 and $(Mo,Cr,W)B_2$ phases (Fig.2f, g). The last zone is of the bulk composite depleted on $MoSi_2$.

A similar structure of contact melting zones was observed for the VH4L-VI-(ZrB_2-15 wt.% $MoSi_2$) couple (Fig. 3). The only difference is the phase composition. The first and second zones with thicknesses of ~ 620 μm and ~ 265 μm, respectively, have practically the same phase compositions; the difference is only in the ratio between the amount of the nickel matrix and reinforcing Cr_2B and intermetallic $(Ni,Cr)_5Zr$ phases

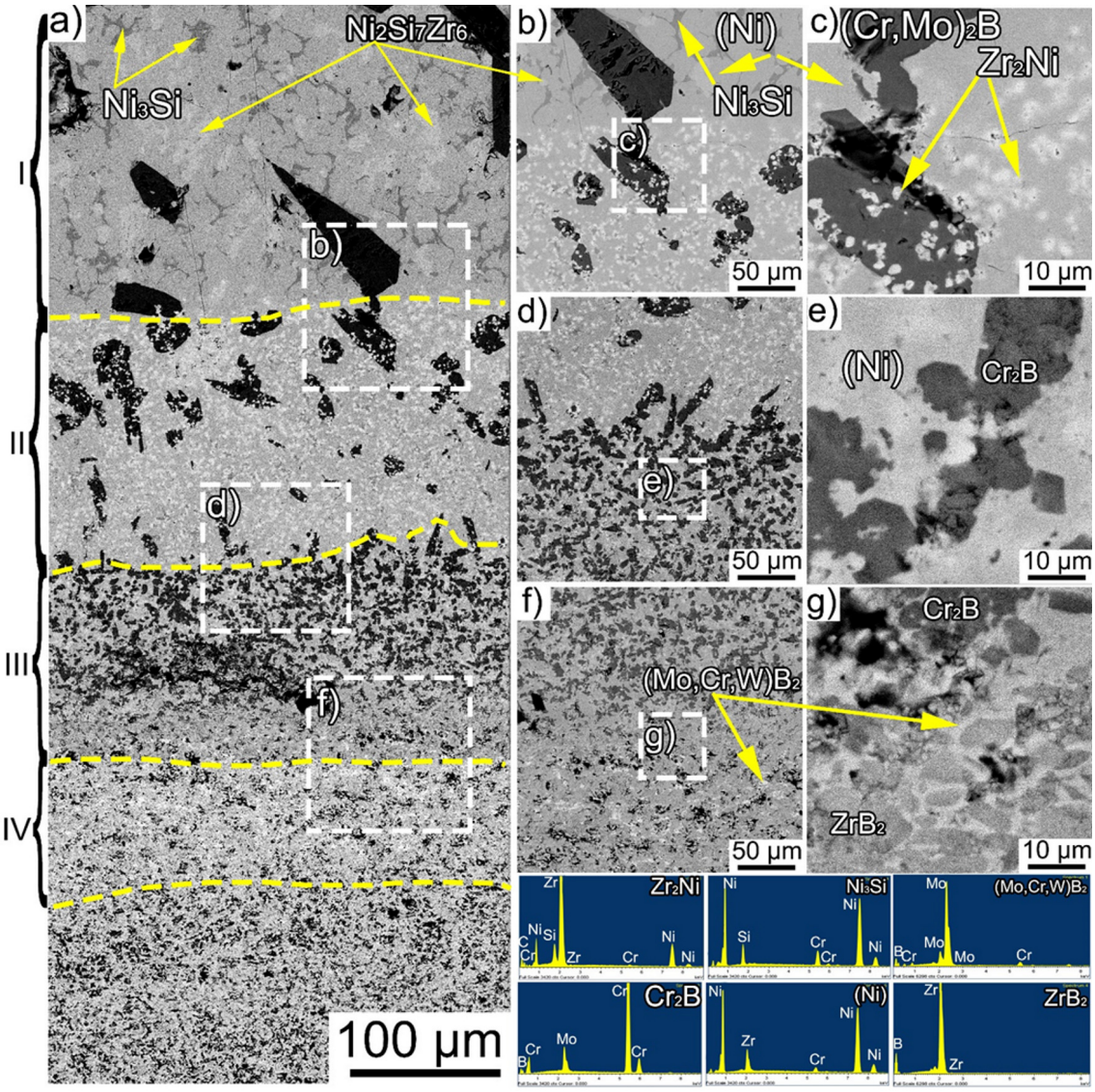

Fig.4. Cross-section microstructure and phase composition of the (NiCr)–(ZrB_2-15 wt. % $MoSi_2$) contact couple after an annealing at 1200°C for 3hours: (a) general view, (b, c) region with Ni3Si, Zr_2Ni and $(Cr,Mo)_2B$ phases, (d, e) intermediate zone with Cr_2B and Ni solid solution, (f, e) zone adjacent to ceramics.

(Fig. 3a, b, c). In the third zone, the main phases are complex chromium-molybdenum diboride $(Mo,Cr)B_2$ and chromium diboride (CrB_2), as well as excess ZrB_2, which did not participate in the interaction (Fig. 3d). The fourth zone with a thickness of ~ 50 μm is zirconium diboride depleted on $MoSi_2$ (Fig. 3e).

The same gradient structure with 4 zones formed over the cross section in the contact of the NiCr-(ZrB_2-15 wt.% $MoSi_2$) couple upon cooling from a temperature more than 1200°C (Fig. 4). The first zone with a thickness of ~ 50 μm is a composite consisting of a nickel matrix reinforced with $Ni_{16}Si_7Zr_6$, Ni_3Si silicides and complex $(Cr,Mo)B_2$ diboride (Fig. 4a, b, c). The second zone with a thickness of ~ 155 μm consists of the previous phases with the addition of Zr_2Ni intermetallic compound and a reduced amount of $Ni_{16}Si_7Zr_6$ and Ni_3Si phases (Fig. 4d, e). The third zone ~ 90 μm thick has the same phase composition, but a changed microstructure (Fig. 4f, g). The amount of chromium boride increases, and it becomes fine-grained (Fig. 4g). The fourth zone with a thickness of 120 μm is a layer of zirconium diboride depleted in molybdenum silicide with a small amount of inclusions of complex $(Mo,Cr,W)B_2$ diboride.

4. Discussion

The solid-state interaction and contact melting of X18H10T, VH4L-VI and NiCr with ZrB_2-15 wt.% $MoSi_2$ were investigated.

It was shown that no interaction with the formation of new phases was observed in the X18H10T-ZrB_2MoSi_2 -15 wt.% $MoSi_2$ system up to 1200°C. Changes occur only in the near-contact zone of the composite; $MoSi_2$ disappears with the formation of pores. We assume that this is due to the high chemical affinity of silicon for iron and nickel [27]. A wide homogeneity range for a solid solution of silicon in iron, a high diffusion rate of Si atoms in the solid solution (at a temperature of 1200°C D_0 = 0.44 cm^2/s; E = 201 kJ/mol [27]) and the possibility of creating silicide phases make iron an active catalyst for the decomposition of $MoSi_2$ at the contact area and diffusion of silicon into iron. This creates a gradient of silicon in the near-contact zone of the composite, which stimulates its delivery from the volume of the alloys. As a result, conditions are created for the decomposition of $MoSi_2$ in deeper layers of the composite ceramics; as well, a porosity zone is formed, the size of which depends on the temperature and time of annealing.

Similar processes during solid-phase interaction also occur in VH4L-VI-(ZrB_2-15 wt.% $MoSi_2$) and NiCr–(ZrB_2-15 wt.% $MoSi_2$) couples. The difference is in the fact that in these systems, in addition to the diffusion of silicon from the composite into the metal, counter-diffusion of chromium from the metal into the contact surface occurs (Fig. 1 b, c). This is possible due to a significant concentration of chromium in the alloys, as well as its high affinity for boron and the rate of diffusion of nickel atoms (at 900°C, D_0 = 0.44 cm^2/s; E = 201 kJ/mol [27]). As a result, part of the chromium entering the contact interface interacts with boron forming the Cr_2B phase. The second part diffuses into the composite and, together with the molybdenum and tungsten remaining after mixing, forms the $(Mo,Cr,W)B_2$ phase, which is concentrated in the porosity.

In fact, MoB_2 boride is formed in the crystal lattice of which some of the molybdenum atoms are replaced by atoms with a similar electronic structure and, accordingly, many properties. This is confirmed by the fact that they are all in the same group of the periodic table. That is, as a result of the solid-phase interaction at the boundary of the contacting phases, new phases are formed. The formation of the new phases can be described by the following reaction equations:

$$ZrB_2 + Cr \rightarrow Cr_2B + Zr, \quad (1)$$

$$MoSi_2 + 4Ni = 2Ni_2Si + Mo, \quad (2)$$

$$MoSi_2 + 6Fe = 2Fe_3Si + Mo, \quad (3)$$

$$Fe_3Si + Zr = Fe_2Si_7Zr_6, \quad (4)$$

$$Ni_3Si + Zr = Ni_2Si_7Zr_6. \quad (5)$$

The formation of $Fe_2Si_7Zr_6$ ($Ni_2Si_7Zr_6$) leads to contact melting, since there is a eutectic between $Ni_2Si_7Zr_6$ and Ni_2Si at a temperature of ~ 1200°C [29].

During contact melting at temperatures above 1200°C, the phase composition and ratio between newly formed phases change over the cross section of the contact zone. In this case, the main phases after interaction are stainless steel alloyed with silicon and zirconium, as well as $(Fe,Cr)_2B$, $Fe_2Si_7Zr_6$, $(Mo,Cr,W)B_2$ and ZrB_2.

Several characteristic zones are formed independent of contact couple. The first zone adjacent to the metal contains Cr_2B formed as a result of solid-phase interaction and intermetallic phases (Fig. 2c, Fig. 3c, Fig. 4i). The intermetallic phases are formed according to the following scheme:

$$ZrB + Cr \rightarrow Cr_2B + Zr; \quad Zr + Ni = Ni_5Zr; \quad Zr+Ni = Zr_2Ni. \quad (6)$$

The existence of one or another intermetallic phase depends on the type of the contact couple and the metal concentration in the alloy.

The second zone is located between pure metal and ceramics (Fig. 2b, d; Fig. 3b; Fig. 4b, d). The phase composition in these regions is more diverse. The main characteristic is the presence of Cr_2B and silicides in each contact couple. Considering the possible reaction equations for the formation of silicides (7–16), one can see that the most favourable is the formation of iron or nickel silicides due to their interaction with molybdenum disilicide — the reaction 2 or 3 and further interaction with zirconium due to the interaction of ZrB_2 with Cr.

$$MoSi_2 + 3ZrB_2 + 8Fe = MoB_2 + 4Fe_2B + Zr + 2ZrSi(+264\ k/mol), \quad (7)$$

$$MoSi_2 + 2ZrB_2 + 4Fe = \quad (8)$$
$$= MoB_2 + 2Fe_2B + Zr + ZrSi_2(+296\ k/mol),$$

$$MoSi_2 + ZrB_2 + 6Fe = \quad (9)$$
$$= MoB_2 + Zr + 2Fe_3Si(+110kJ/mol)'$$

$$MoSi_2 + ZrB_2 + 2Fe = \quad (10)$$
$$= MoB_2 + Zr + 2FeSi(+176kJ/mol),$$

$$MoSi_2 + ZrB_2 + Fe = \quad (11)$$
$$= MoB_2 + Zr + FeSi_2(+260kJ/mol),$$

$$MoSi_2 + 1.5ZrB_2 + 3Fe = \quad (12)$$
$$= MoB_2 + 1.5Zr + FeSi_2 + Fe_2B(+260kJ/mol),$$

$$MoSi_2 + 2ZrB_2 + 4Ni = \quad (13)$$
$$MoB_2 + 2Ni_2B + 2ZrSi(+193kJ/mol),$$

$$MoSi_2 + ZrB_2 + 4Ni = \quad (14)$$
$$= MoB_2 + Zr + 2Ni_2Si(+60kJ/mol),$$

$$MoSi_2 + ZrB_2 + 2Ni = \quad (15)$$
$$= MoB_2 + Zr + 2NiSi(+145kJ/mol),$$

$$MoSi_2 + ZrB_2 + Ni = \quad (16)$$
$$= MoB_2 + Zr + NiSi_2(+227kJ/mol).$$

Therefore, approaching ceramics, the' amount of silicides is significant due to the high silicon content.

The third layer adjacent to the ceramics preferably consists of ZrB_2 and Cr_2B phases. It should be noted that more chromium in the alloy resulted in the formation of more Cr_2B. The formed Cr_2B reduces the diffusion of other elements into the diffusion zone and the interaction zone becomes smaller. This is confirmed by the formation of a thinner interaction zone for the VH4L-VI-(ZrB_2-15 wt. % $MoSi_2$) (~ 800 μm) couple than for the (NiCr)-(ZrB_2-15 wt. % $MoSi_2$) (~ 500 μm) couple, as well as by the formation of nickel-rich intermetallic compounds (Ni_5Zr), due to the small amount of zirconium.

A common feature of the studied systems is that the temperature of their contact melting is significantly lower than the melting temperature of the contacting materials themselves (ZrB_2 — 3200°C; $MoSi_2$ — 2030°C; X18H10T — 1480°C; VH4L-VI — 1455°C; Ni–20Cr — 1450°C). This means that they are on the line of intersection of multicomponent state diagrams with eutectic points. This is confirmed by the data of [29], where it is shown that the eutectic composition Ni_2Si–$Ni_{16}Si_7Zr_6$ is present in the Zr–Ni–Si system at a temperature of 1200°C. However, the Zr–Ni–Si system is actually a part of a more complex Zr–Ni–B–Si–Cr(Mo) system, one of the sections of which contains part of the alloys under study.

Based on the studies, contact couples X18H10T-(ZrB_2-15 wt. % $MoSi_2$), VH4L-VI-(ZrB_2-15 wt. % $MoSi_2$), (NiCr)-(ZrB_2-15 wt. % $MoSi_2$) can operate at temperatures not exceeding 1000°C, in the designs of fuel equipment and other flame devices that are in long-term operation. More intensive regimes, with temperatures of 1200°C and higher, require the creation of barrier layers at the contact boundary, which exclude the possibility of diffusion interaction leading to contact melting of materials.

5. Conclusion

1. It is shown that up to temperatures of 1200°C in the contact couple of ZrB_2-15 wt.% $MoSi_2$-alloys based on nickel and iron, solid-phase interaction results in the formation of a new Cr_2B phase and diffusion of silicon into the metal.

2. At temperatures above 1200°C, contact melting occurs due to the formation of low-melting eutectics in the Ni–Zr–Si–B–Cr systems.

References

1. F.J.Justin, A.J.Jankowiak, J.F.Justin, *Aerosp. Lab J.*, **8**, 1 (2011).
2. W.G.Fahrenholtz, E.J.Wuchina, W.E.Lee, Y.Zhou, Ultra-High Temperature Ceramics Materials for Extreme Environment Applications, John Wiley & Son (2014).
3. S.C.Zhang, G.E.Hilmas, W.G.Fahrenholtz, *J. Am. Ceram. Soc.*, **94**, 1198 (2011). https://doi.org/10.1111/j.1551-2916.2010.04216.x.
4. D.M.Kazemzadeh, W.G.Fahrenholtz, G.E.Hilmas, *Corros. Sci.*, **91**, 224 (2015). https://doi.org/10.1016/j.corsci.2014.11.019.
5. D.M.Kazemzadeh, W.G.Fahrenholtz, G.E.Hilmas, *J. Eur. Ceram. Soc.*, **33**, 1591 (2013). https://doi.org/10.1016/j.jeurceramsoc.2013.01.033.
6. L.Silvestroni, H.J.Kleebe, W.G.Fahrenholtz, *J. Watts, Sci. Rep.*, **7**, 1 (2017). https://doi.org/10.1038/srep40730.
7. P.Hu, Z.Wang, *J. Eur. Ceram. Soc.*, **30**, 1021 (2010). https://doi.org/10.1016/j.jeurceramsoc.2009.09.029.
8. N.Gilli, J.Watts, W.G.Fahrenholtz et al., *Compos. Part B Eng.*, **226**, 344 (2021).

https://doi.org/https://doi.org/10.1016/j.compositesb.2021.109344.

9. O.N.Grigoriev, I.P.Neshpor, T.V.Mosina et al., *Powder Metall Met Ceram.*, **56**, 573 (2018). https://doi.org/10.1007/s11106-018-9930-z
10. L.Silvestroi, H.J.Kleebe, S.Lauterbach et al., *J. Mater. Res.*, **25**, 828 (2010). https://doi.org/10.1557/jmr.2010.0126.
11. R.J.Grohsmeyer, L.Silvestroni, G.E.Hilmas et al., *J. Eur. Ceram. Soc.*, **39**, 1939 (2019). https://doi.org/10.1016/j.jeurceramsoc.2019.01.022
12. F.Monteverde, R.J.Grohsmeyer, A.D.Stanfield et al., *J. Alloys Compd.*, **779**, 950 (2019). https://doi.org/10.1016/j.jallcom.2018.11.238.
13. D.Sciti, L.Silvestroni, M.Nygren, *J. Eur. Ceram. Soc.*, **28**, 1287 (2008). https://doi.org/10.1016/j.jeurceramsoc.2007.09.043.
14. D.Sciti, S.Guicciardi, A.Bellosi, G.Pezzotti, *J. Am. Ceram. Soc.*, **89**, 2320 (2006). https://doi.org/10.1111/j.1551-2916.2006.00999.x.
15. L.Silvestroni, G.Meriggi, D.Sciti, *Corrosion Science.*, **83**, 281 (2014). https://doi.org/10.4018/978-1-4666-4066-5.ch005.
16. D. Vedel, A. Osipov, L. Melakh et al., *J. Eur. Ceram. Soc.* **43**, 3025. (2023).
17. L.Silvestroni, K.Stricker, D.Sciti, H.J.Kleebe, *Acta Mater.*, **151**, 216 (2018).
18. N.Rao, *Adv. Gas Turbine Technol.*, (2011). https://doi.org/10.5772/20730.
19. D.G.Backman, J.C.Williams, *Science*, **80**, 1082 (1992). https://doi.org/10.1126/science.255.5048.1082.
20. G.L.Zhunkovskii, O.M.Grigoriev, D.V.Vedel, *J. Superhard Mater.*, **44**, 102 (2022). https://doi.org/10.3103/S1063457622020095
21. G.L.Zhunkovskii, T.V.Mosina, I.P.Neshpor et al., *Powder Metall Met Ceram.*, **57**, 551 (2019). https://doi.org/10.1007/s11106-019-00014-x
22. G.L.Zhunkovskii, T.V.Mosina, I.P.Neshpor et al., *Powder Metall Met Ceram.*, **57**, 647 (2019). https://doi.org/10.1007/s11106-019-00027-6
23. O.N.Grigoriev, H.L.Zhunkovski, D.V.Vedel, V.A.Kotenko, *Powder Metall Met Ceram.*, **58**, 455 (2019). https://doi.org/10.1007/s11106-019-00095-8
24. A.Panasyuk, V.Fomenko, L.Glebov, Stability of Non-metallic Materials in Melts, Naukova Dumka (1986) [in Ukraine].
25. P.Sebo, P.Svec, M.Zemankova et al., *Kov. Mater.*, **52**, 321 (2014). https://doi.org/10.4149/km_2014_6_321.
26. G.L.Zhunkovsky, T.M.Evtushok, O.N.Grigoriev et al., *Powder Metallurgy.*, No.3/4, 109 (2011).
27. G.V.Samsonov, Physical and Chemical Properties of Elements, Naukova Dumka (1965) [in Ukraine].
28. G.V.Samsonov, I.M.Vinitsky, Refractory Compounds. Directory. 2nd ed., Metallurgy, Moscow (1976) [in Russian].
29. M.Xiao, Y.Du, K.Xu et al., *J. Phase Equilibria Diffus.*, **41**, 615 (2020). https://doi.org/10.1007/s11669-020-00826-0